Steel and Composite Structures, *Vol. 27, No. 6 (2018) 675-689*
DOI: https://doi.org/10.12989/scs.2018.27.6.675

Buckling-restrained brace with CFRP encasing: Mechanical behavior & cyclic response

S. Ali Razavi *, Amirhossein Kianmehr, Abdollah Hosseini and S. Rasoul Mirghaderi

Faculty of Civil Engineering, University of Tehran, Tehran, Iran

(*Received June 12, 2016, Revised March 2, 2017, Accepted April 17, 2018*)

Abstract. Buckling-restrained braces (BRBs) have received considerable attention in seismic design of various types of structures. Conventional BRBs are composed of steel core and surrounding steel tube filled with concrete. Eliminating the steel tube can be advantageous to BRB. In this study the idea of replacing the steel tube by CFRP layers in BRBs is proposed. The advantages of this type of BRB are mentioned, and its design criteria are introduced. The construction procedure of two BRB specimens is described. The specimens are uniaxially tested based on moderate, and severe earthquake levels and the performance of the specimens is investigated. The backbone curves resulted from the hysteresis curve are presented for the design proposes. The results of this study show that CFRP layers can effectively provide the expected performance of the encasing, and the proposed BRB can be considered a viable alternative to the conventional BRBs.

Keywords: buckling-restrained brace; CFRp layers; cyclic test; design criteria

1. Introduction

Nowadays buckling-restrained braces (BRBs) are frequently used in building and bridge construction. Besides high stiffness, BRBs provide high energy dissipation capacity and high ductility. Typical BRBs consist of a steel core, encasing and debonding material. The behavior of BRB in tension and compression is approximately similar due to the presence of encasing which prevents global buckling of the brace and restrains the local buckling of the core. Encasing is normally a hollow steel section (HSS) filled with concrete. Numerous researches have been conducted on using alternative materials for encasing, such as steel (Park *et al*. 2012, Tremblay *et al*. 2006) and fiber reinforced polymer (FRP) materials (Dusicka and Wiley 2008).

1.1 Research motivation

BRBs are composed of steel core and encasing which is typically made of a concrete filled steel tube. The steel tube of the encasing should be stiff enough to restrain the out-of-plane actions generated by the core. In design of the steel tubes for concrete filled encasings, the out-of-plane strength defines the size and thickness of the tube. This often leads to a heavy encasing. Observations have shown that disregarding the out-of-plane demands on the steel tube results in its local failure and bulging (Chou and Chen 2010, Lin *et al*. 2011). Since the encasing tube is prone to slip on concrete, the composite action between the tube and concrete is not fully mobilized. Therefore normally the global stability of the brace is checked considering the flexural stiffness of the steel tube (Uang and Nakashima 2004, Black *et al*. 2002). Concrete which comprises the major weight of the brace acts as filler, besides being the first interface to locally resist the normal forces exerted by the steel core. Hence, in typical BRBs concrete and steel are used in an unpredictable composite action which increases the weight of the brace.

In conventional BRBs the concrete is poured in an enclosed section, therefore observing concrete during pouring process and vibrating may not be accomplished satisfactorily, which in turn leads to special considerations for assuring about the concrete workability and homogeneity.

Recent studies show that the normal force induced by core is not uniform through the length of BRB (Tabatabaei *et al*. 2014); this leads to variable demand for flexural stiffness and strength in different zones of encasing. The maximum demand induced by the core governs the design of encasing. If a uniform section is used in the length of encasing the demand to capacity ratio cannot be adjusted leading to an uneconomical encasing. So from the economic point of view, being able to adjust the strength in different parts of encasing according to the demand can be beneficial.

Considering the aforementioned disadvantages of typical BRBs, proposed in this paper, the outer steel tube is eliminated and two sandwiching precast concrete blocks are utilized to provide the stability of the brace. This objective is implemented by using carbon FRP (CFRP) layers wrapped around the concrete blocks.

FRP material has extremely high strength to weight ratio in comparison to steel. Gluing CFRP layers to concrete mobilizes the composite action completely and enables effective use of concrete material to restrain the global and local buckling with less weight compared to typical BRB

*Corresponding author, Ph.D.,
E-mail: arazavi@ut.ac.ir

ISSN: 1229-9367 (Print), 1598-6233 (Online)

systems. Furthermore, since the encasing strength is provided by CFRP, in parts of encasing which endure greater out-of-plane loads, more transverse layers can be provided to reach a more cost-effective brace. Another advantage of the CFRP-BRB is the prefabrication of the encasing. This provides a smooth contact surface and a straight alignment for the encasing which in turn enables accurate adjustment of the gap between the two encasing blocks. Tuning the gap and its uniformity is one of the important parameters to attain satisfactory performance for the BRB.

CFRP layers are laid longitudinally and transversely on the concrete encasing. The longitudinal layers of CFRP are designed to provide the flexural rigidity and longitudinal bending strength, while the transverse layers are designed to prevent the core local buckling and provide transverse bending strength. The concept of applying FRP composites in structural members has received considerable attention in rehabilitation strategies and its efficiency has been repeatedly documented (Su *et al*. 2016, Kakaletsis 2016, Wang and Shao 2014), nevertheless, applying CFRP in BRBs is relatively unprecedented.

1.2 Research background

Limited researches are conducted about application of CFRP in BRBs. In an experimental and numerical study, Ekiz and El-Tawil (2008) intended to enhance the compression behavior of steel columns using cement mortar jackets. The weak steel element was surrounded by blocks and then wrapped by CFRP layers to provide adequate lateral constraint for the steel element in order to prevent global buckling and ensure yielding in compression. The small-scale specimens were 500 mm long and all the specimens were loaded monotonically in compression up to failure. The number of longitudinal layers was variable, while a single layer was applied transversely. Unlike the concept of BRBs, in most of the specimens the jacket and CFRP layers completely contribute in resisting compressive load. The results of this study showed that increasing the number of longitudinal layers leads to more stable behavior and larger axial displacement capacity. Specimens with sufficient number of longitudinal layers (more than 4 layers) experienced strains of 3.3-4.6% without global buckling. The failure mode in these specimens was crush in the mortar and failure of transverse fibers at the end of specimen. Also as an important result, bonding fibers to jacket made the encasing stable and debonding jacket from steel core delayed the global buckling of the specimen.

Although the efforts of Ekiz and El-Tawil proved the efficiency of CFRP layers in postponing the global buckling of the axial members, significant issues such as the detail of debonding steel member from the jacket, the detail of holding the jackets to steel, and the effects of cyclic loads have not been addressed. Moreover, the design criteria for longitudinal and transverse CFRP layers are not presented.

This study was continued by conducting large-scale tests on real braces. The proposed strengthening strategy improved the performance of the braces up to drift of 2%; however, El-Tawil and Ekiz (2009) considered this system appropriate for resisting wind loads and cases which the nonlinear behavior of the brace is not expected. They recommended enhancing this strengthening strategy prior to applying in the high seismic zones.

In another study aimed at decreasing the weight of BRB, Dusicka and Wiley (2008) proposed pultruded FRP tube which restrained an A36 L-shaped core by wrapping GFRP around the FRP tube and the core. In this research silicon layers were used on steel surface to decrease the friction between the core and the FRP tube. Behavior of specimen was reported satisfactory, but the L-shaped sections fractured in the transition area at one end of encasing due to the formation of plastic hinge. The proposed idea inhibited the global buckling of the brace and guided the failure to yielding of the core near the connection. The formation of plastic hinge caused an increased load in GFRP layers which caused its rupture.

For the time being, research on BRBs with FRP wrapped encasings is demanded. This study presents the design basics of BRB with concrete encasing wrapped with CFRP. A building using BRB as the lateral resisting system is designed and based on the design results BRB specimens are detailed, constructed, and experimentally tested and the performance of the CFRP-BRB is evaluated and described.

2. Introduction to design basics of CFRP-BRB

2.1 Mechanical behavior

The CFRP-BRB is composed of steel core, two precast concrete blocks and CFRP layers wrapping around the blocks. Concrete acts as the elastic restraint for the core and allows it to buckle in higher modes during compressive yielding. The stiffness of concrete prevents the local buckling of the core. CFRP layers are arranged in longitudinal and transverse direction in order to support the concrete encasing. The CFRP-wrapped encasing holds the key role in providing the global stability.

2.2 Design basics

When the steel core yields, the brace and its components endure local and global actions. A criterion is developed for each action which will be described in the following sections.

2.2.1 Global buckling

The brace must preserve its stability when the core yields or reaches its maximum compressive load. This criterion is checked by the well-known Watanabe *et al*. (1988) formulation. In CFRP-BRB, the buckling capacity of the brace is calculated by considering the encasing concrete blocks. The construction provisions usually lead to relatively massive concrete blocks and subsequently adequate buckling capacity is provided. Therefore this criterion is simply satisfied and rarely governs the design of CFRP-BRB.

2.2.2 Flexural stability of encasing

Presence of gap between the core and encasing and the probable eccentricities exerts a P-δ bending on the brace as

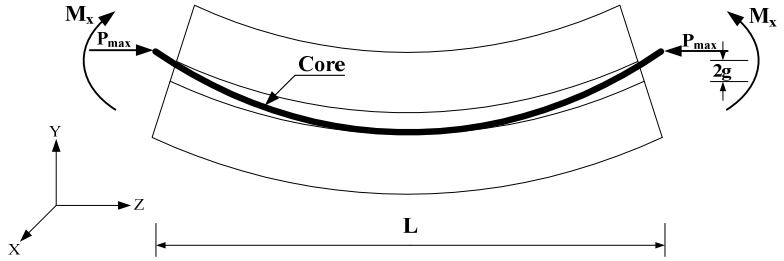

Fig. 1 Development of flexure in encasing due to the *P-δ* effect

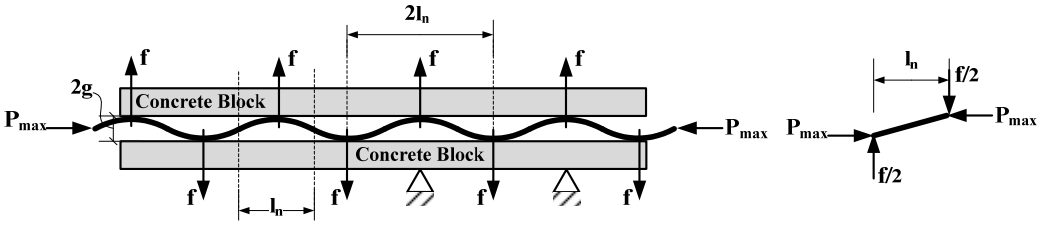

Fig. 2 Deformed core and normal forces on encasings

shown in Fig. 1. This bending moment should be resisted by encasing.

The formulation of this criterion is adopted from ACI 318 (2014) based on the recommendation of Nilson *et al*. (2010)

$$\frac{P_{\max,C}\delta_{\max,y}}{M_{cx}}+\frac{P_{\max,C}\delta_{\max,x}}{M_{cy}}\le 1 \tag{1}$$

Where M_{cx} and M_{cy} are the flexural capacity of encasing including two concrete blocks about weak and strong axis of the core, respectively. $\delta_{\max,x}$ and $\delta_{\max,y}$ are the total in-plane and out-of-plane eccentricities that include out of straightness at the middle of the brace, eccentricities at the beginning and end of the brace, self-weight deflection and amplification of the sum of abovementioned displacements in compression loads. The cumulative amount of eccentricities is estimated to be L/150 according to Razavi *et al*. (2011) in which *L* is the length of encasing.

2.2.3 Clamping force in the side legs of encasing

As a result of higher mode buckling the core exerts local force on the encasing. Fig. 2 illustrates the deformed shape of the core and normal forces acting on the encasing (*f*).

The equilibrium equation of moments for the free-body diagram in Fig. 2 gives the normal force as follows

$$f=4P_{\max,C}\frac{g}{l_n} \tag{2}$$

Where *g* is the gap between the core and the encasing in one side (the total gap is 2*g*), l_n is the wavelength of the higher mode buckling.

Genna and Gelfi (2012a) conducted an experimental research on estimating the wavelength of buckled core in higher modes. This research was followed by a parametric study using finite element analyses which showed

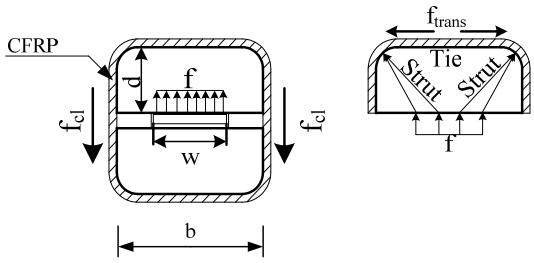

Fig. 3 Developing of local forces in encasing of CFRP-BRB

appropriate compatibility with the test results. According to experimental and numerical results, engineering equations were developed in order to calculate the wavelength and normal load of the core considering the effects of friction, core plasticity and repeated cycles of loading (Genna and Gelfi 2012b). In this study the equation developed by Genna and Gelfi is used to estimate l_n (Eq. (39) in Genna and Gelfi 2012b).

The normal force of core tends to detach two concrete blocks and as a result the CFRP wrapped around encasing experience tensile stress. Fig. 3 illustrates the clamping stress (f_{cl}) in the side legs of the encasing.

As shown in Fig. 2 the effective length which endures the clamping force is twice as the buckled core wavelength. Accordingly the tensile stress of the CFRP layers is calculated as follows

$$f_{cl}=\frac{f}{4l_n t} \tag{3}$$

Where *t* is the total thickness of CFRP layers in each side leg of encasing.

2.2.4 Local strut and tie action

In order to investigate the local strut and tie action, one can assume an individual block as a simply supported beam

with uniform loading in the middle (Fig. 3). The depth of the block (d) is large with respect to its width (b), hence it would be a deep beam. In this deep beam, the normal force of the core causes local strut and tie action in the transverse direction of the concrete block (Fig. 3). Due to this action a tensile stress is developed on the tie leg of a deep beam with length of b, depth of d and width of $2l_n$ which can be formulated by the following equation

$$f_{trans} = \frac{2b - w}{16 l_n dt} f \tag{4}$$

Where w is the width of steel core.

By considering the abovementioned design criteria the encasing of the CFRP-BRB is designed.

3. Test plan and properties of the specimens

In order to evaluate the performance of the CFRP-BRB experimentally, a brace of a designed building is selected to be detailed and manufactured. Properties and design details of the building will be introduced in the following section.

3.1 Building design and descriptions

Plan of a six story residential building is shown in Fig. 4. This building has five spans of 5 m in X direction and four spans of 4 m in Y direction. The height of all stories is 3.2 m. The lateral resisting system of the structure in both directions is inverted-V BRBs. The brace location in the plan of building is shown in Fig. 4. The seismicity parameters proposed by ASCE 7 (2010) are used to estimate the seismic load. The building is located on site class C and seismic category D. Response modification factor (R) of 8, overstrength factor (Ω_d) of 2.5 and displacement amplification factor (C_d) of 5 are selected.

The structure is designed according to AISC 341 (2010) and the results of design in X direction are presented in Table 1.

Table 1 Design results of bracings in x direction

Story	F_d	w	t	A	F_{cap}	F_d/F_{cap}
	kN	mm	mm	mm^2	kN	
6	212	90	12	1080	229	0.93
5	334	120	15	1800	381	0.88
4	438	120	20	2400	509	0.86
3	505	140	20	2800	593	0.85
2	554	140	20	2800	593	0.93
1	500	140	20	2800	593	0.84

In Table 1, F_{cap} and F_d are brace axial load capacity and demand, respectively. Parameters b, t and A are the width, thickness and area of the core cross section, respectively.

Brace of the third story on axis 1 are half-scaled for experimental purpose. Based on the results of analysis the design inter story drift of this story is 1.55%.

3.2 Design and detailing of the specimens

Two specimens are designed to be tested. Both specimens are identical, except the loading protocol, end connections, and CFRP properties. In order to investigate the performance of the proposed BRB in ground motions stronger than the design basis earthquake (DBE), specimen 2 is studied for the displacement amplitudes corresponding to the maximum considered earthquake (MCE).

The core is made of ST 37-2 steel (DIN) with yield strength of 248 MPa, ultimate strength of 402 MPa and strain hardening factor of 62%. The core is made of a rectangular section of 70 mm width and 10 mm thickness. The width of the core increases in a transition length and two 10 mm stiffener plates perpendicular to the core are provided at the end of the core. Eight holes are drilled on each end of specimen 1 to connect the specimen to the test setup. In Fig. 5 the top and side views of specimen 1 is depicted.

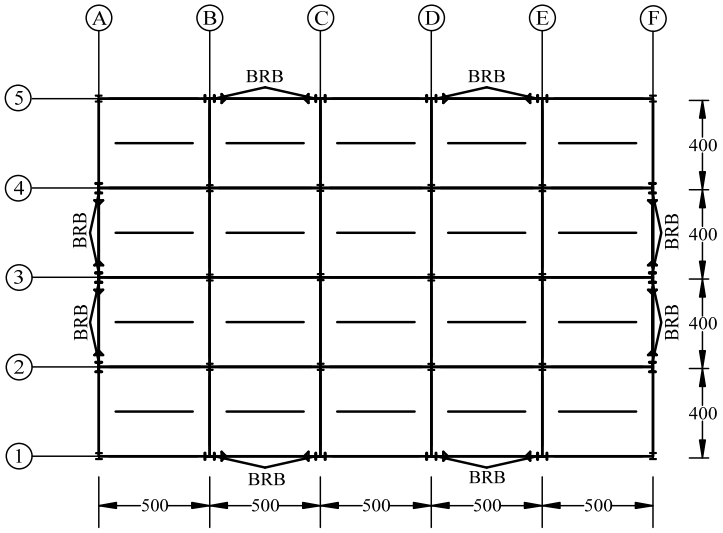

Fig. 4 Plan of the six story building

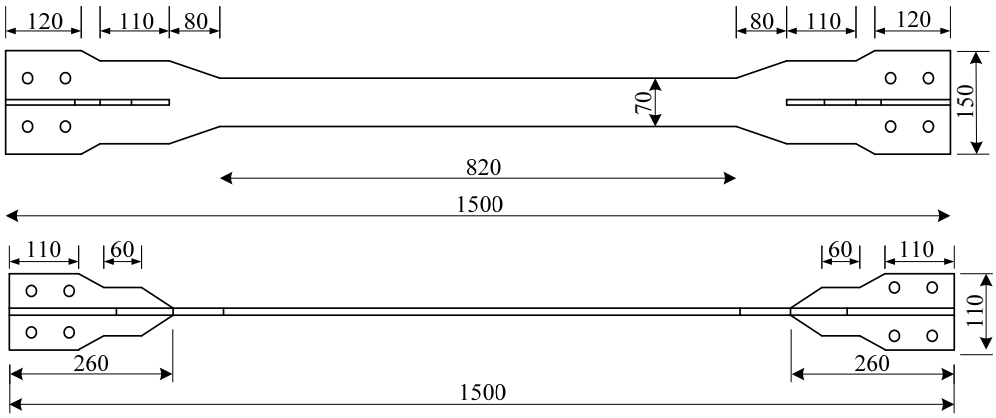

Fig 5 Detailing of the core (specimen 1)

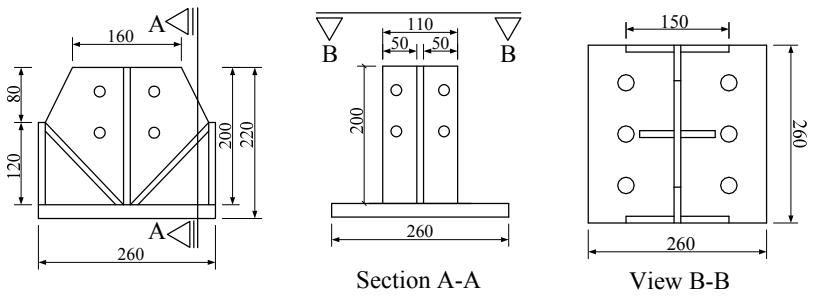

Fig. 6 Detailing of the connection head (specimen 1)

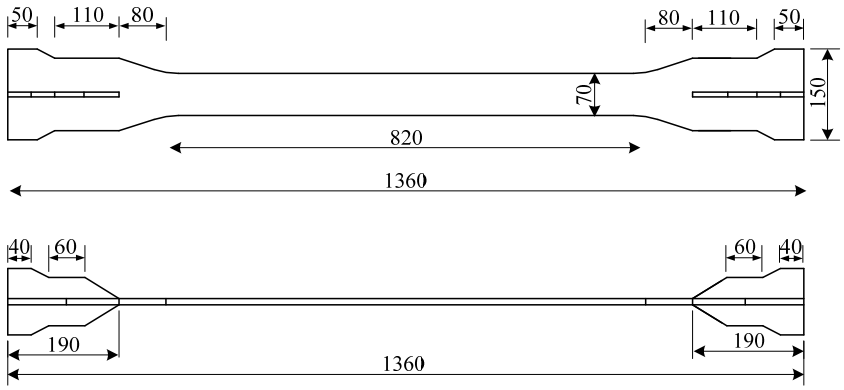

Fig. 7 Detailing of the core (specimen 2)

To connect specimen 1 to the test setup, a special connecting head is used which is composed of two main plates and 10 stiffeners as shown in Fig. 6.

The core is connected to the connection head using four splice plates and 16 M16 high strength 12.9 (European grade) bolts. Bolts are pretensioned to ensure friction. The whole length of specimen considering the connection head is 1960 mm.

In contrast to specimen 1, complete joint penetration (CJP) groove weld is used to connect specimen 2 to two 30 mm end plates. In this method the time consuming operation of adjusting the holes and fastening the bolts is eliminated, furthermore the connection length is decreased. The whole length of specimen considering the end plates is 1420 mm. The detailing of the core of specimen 2 is shown in Fig. 7.

The connection head and end plates are bolted to top and bottom plates of uniaxial loading setup using high strength bolts.

Encasing consists of two prefabricated concrete blocks, steel filler plates on edges, and CFRP layers. The advantage of prefabricated encasing in contrast with concrete-filled steel tubes is that the contact surface of the encasing is visible and at hand; hence any unevenness and roughness can be smoothed prior to assembling the BRB parts. Moreover, since this surface is accessible it can be easily painted by the debonding material. Due to the smooth surface of encasing and the use of steel filler plates with precise thickness, the gap between the core and encasing can be adjusted accurately.

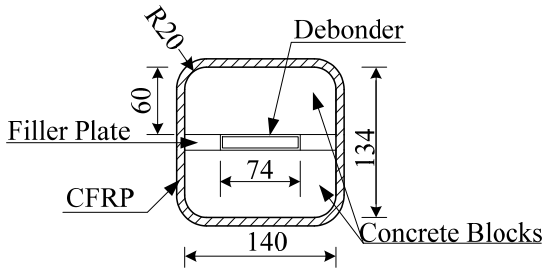

Fig. 8 Section of CFRP-BRB

The concrete mix is designed to reach compressive strength of 55 MPa. This strength grade provides appropriate stiffness and elasticity for limiting local buckling and can mobilize the core buckling in higher modes. Superplasticizers are used in the mix design to provide proper workability and smooth finished surface.

In specimen 1 CFRP layers with nominal thickness of 0.117 mm for each layer are used. The ultimate tensile strength, elastic modulus and rupture strain of CFRP layers are 4116 MPa, 240 GPa and 1.72%, respectively.

The width and height of each encasing block is selected 140 mm and 60 mm, respectively. The corners of encasing are curved with a 20 mm radius to enhance the effect of CFRP layers. The section of the assembled blocks is depicted in Fig. 8.

Considering the required longitudinal gap between the core and the encasing to prevent the contact of the end of stiffener to concrete, the length of encasing is selected 1150 mm. The configuration of the encasing with respect to the core and end plates of specimen 1 and specimen 2 is shown in Figs. 9 and 10, respectively.

According to ACI 440.2 (2008) and the properties of CFRP layers used in specimen 1 and the dimensions of the encasing, the demand/capacity ratio of the design criteria is listed in Table 2.

As higher displacement amplitudes are applied to specimen 2, higher compressive strain is induced and as a result the wavelength of higher mode buckling would be

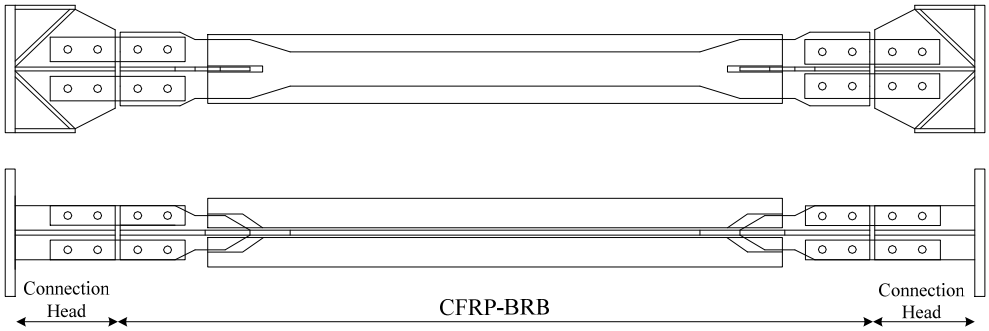

Fig. 9 The configuration of the encasing to the core (specimen 1)

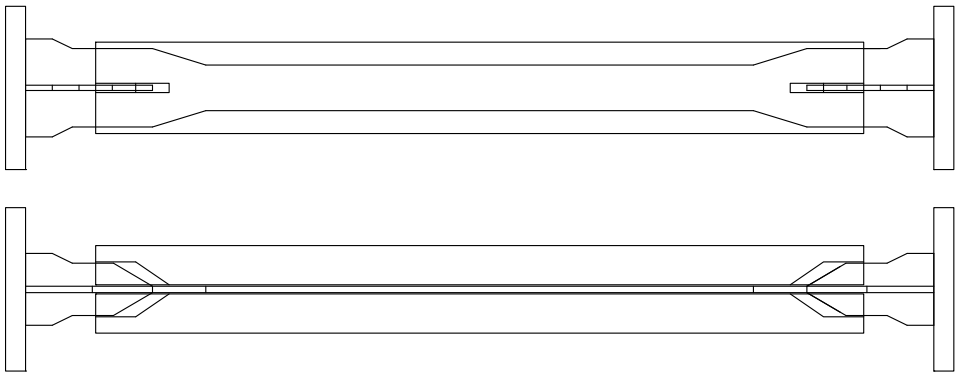

Fig. 10 The configuration of the encasing to the core (specimen 2)

Table 2 The design properties of specimen 1

Criteria	Unit	Demand	Capacity	Layer orientation	Number of layers	D/C
Global stability of the brace	kN	386.99	2522.87	Longitudinal	3	0.15
Global bending about weak axis of core	kN-m	5.06	13.34	Longitudinal	3	0.38
Global bending about strong axis of core	kN-m	5.06	13.69	Longitudinal	3	0.37
Clamping force	kN	30.78	116.59	Transverse	3	0.26
Local transverse strut and tie action	kN	13.47	58.29	Transverse	3	0.23

Table 3 The design properties of specimen 1

Criteria	Unit	Demand	Capacity	Layer orientation	Number of layers	D/C
Global stability of the brace	kN	386.99	2522.87	Longitudinal	3	0.15
Global bending about weak axis of core	kN-m	3.53	15.68	Longitudinal	3	0.23
Global bending about strong axis of core	kN-m	3.53	16.10	Longitudinal	3	0.22
Clamping force	kN	34.23	156.00	Transverse	3	0.22
Local transverse strut and tie action	kN	14.98	78.00	Transverse	3	0.19

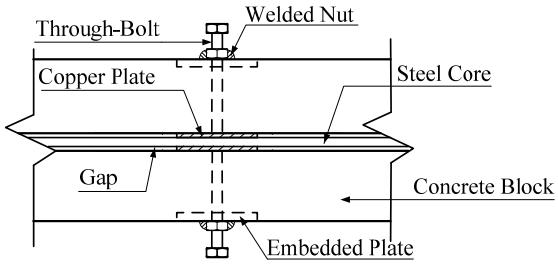

Fig. 11 The stopper mechanism

smaller. To use limited number of wrapping layers in specimen 2, CFRP layers with nominal thickness of 0.176 mm are used. Other mechanical properties of CFRP are the same as specimen 1. The design demand/capacity ratio of encasing of specimen 2 are tabulated in Table 3.

To provide the gap between the core and the encasing two steel filler are used (Fig. 12(b)). Thickness of these fillers is selected 14 mm that provides a 1 mm gap between each encasing block and the core. These fillers are detailed for a 2 mm gap between the core and encasing in the plane of the core.

To hold the encasing to the core the stopper mechanism recommended by Tabatabaei *et al*. (2014) is used. This detailing is based on placing a copper plate between the core and the encasing and an embedded steel plate in encasing block. By fastening two through-bolts, friction between copper plate, steel core and embedded plate is mobilized which ties the encasing to the center of the specimen. The applied detailing for the stopper is shown in Fig. 11.

To prevent friction in the compressive displacements, the inner surface of the encasing is painted by a special 1 mm thick ceramic paste. The porous and rough surface of concrete provides fine adherence for the ceramic paste to prepare a leveled and smoothed finishing. The surface of the core is wrapped with polyethylene tape. Finally both

(a) Concrete blocks

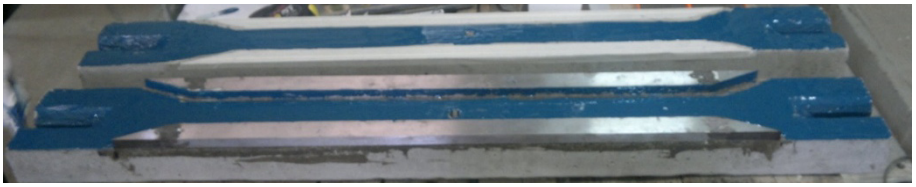

(b) Painting ceramic paste on the inner surface of encasing

(c) The core of a CFRP-BRB

Fig. 12 Construction procedure of specimens

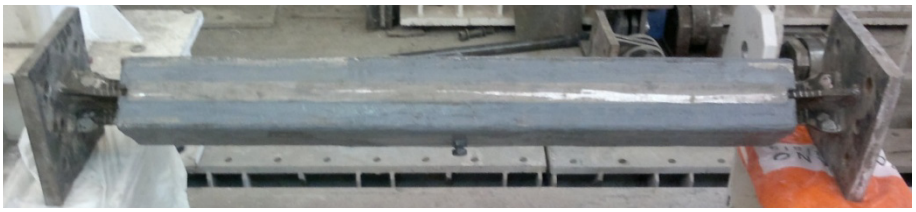

(d) Assembled BRB after covering concrete blocks with resin-based primer

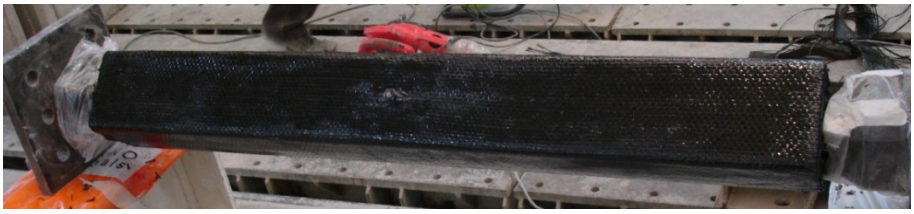

(e) Wrapping CFRP layers over the concrete encasing

Fig. 12 Continued

Table 4 Loading protocol of specimen 1

Cycle amplitude	Unit	Δ_{by}	$0.5\Delta_{bm}$	Δ_{bm}	$1.5\Delta_{bm}$	$2\Delta_{bm}$
Number of cycle	-	2	2	2	2	2
Story drift (Δ/h)	%	0.14	0.78	1.55	2.33	3.10
Story disp. (Δ_m)	mm	4.38	24.80	49.60	75.56	99.2
Scaled BRB disp. (Δ_{bm})	mm	1.35	7.63	15.27	22.90	30.54
$\eta = \sum\Delta_{pl}/\Delta_y$	-	0	37	120	247	420

surfaces of core and encasing are lubricated with grease. The construction process of the specimens is shown in Fig. 12.

3.3 Loading protocol

The loading protocol is developed according to AISC 341 (2010). The loading protocol of specimen 1 represents amplitudes corresponding to DBE level. The design story drift was calculated 1.55% for DBE level. The story displacement of the prototype building is calculated by multiplying 3200 mm by the story drift. By projecting the half-scale value of story displacement on the brace axis, the scaled brace displacement representing the design earthquake (Δ_{bm}) would be 15.27 mm. Dividing the yield force of the specimen by the elastic axial stiffness of the core gives a yield displacement of 1.35 mm. The loading protocol of specimen 1 is given in Table 4.

Specimen 2 is subjected to displacements representing MCE level. According to recommendation of ASCE 41 (2013) the design displacement for MCE level can be considered twice as the displacement calculated for DBE level. Thus in the loading protocol of specimen 2 the brace displacement corresponding to MCE level (Δ_{bm}) is selected two times that of specimen 1. The displacement cycles are applied to the specimens quasi-statically.

3.4 Instrumentations and test setup

Experiments are conducted in a uniaxial loading setup.

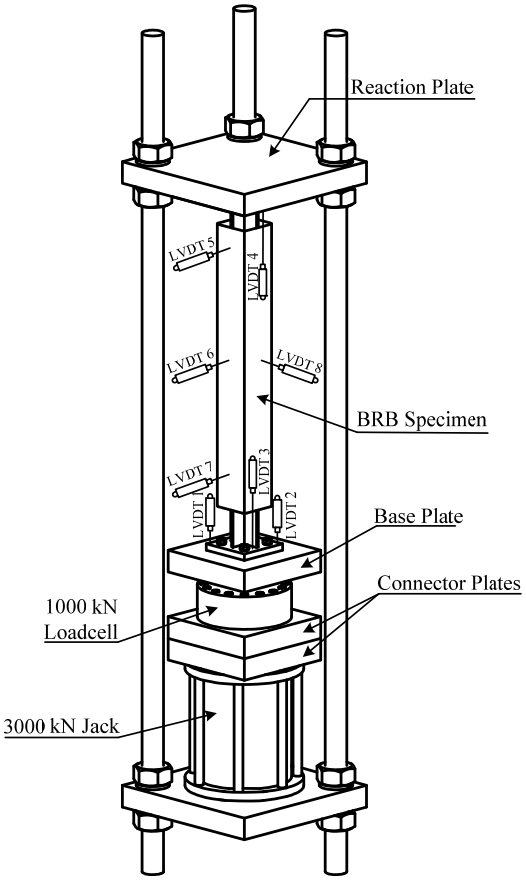

Fig. 13 Test setup

Table 5 Properties of LVDTs installed on the specimen

Sensor No.	Location	Target	Properties
LVDT 1	South	Relative displacement of specimen ends	200 mm gauge
LVDT 2	North	Relative displacement of specimen ends	300 mm gauge
LVDT 3	Top	Distance of encasing from the specimen end plate	50 mm gauge
LVDT 4	Bottom	Distance of encasing from the specimen end plate	50 mm gauge
LVDT 5	Top	Out-of-plane displacement of specimen	25 mm gauge
LVDT 6	Middle	Out-of-plane displacement of specimen	25 mm gauge
LVDT 7	Bottom	Out-of-plane displacement of specimen	25 mm gauge
LVDT 8	Middle	In-plane displacement of specimen	25 mm gauge

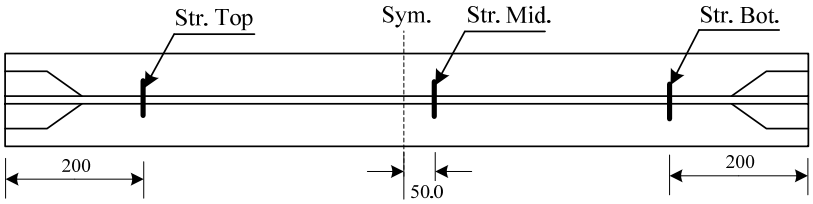

Fig. 14 Location of strain gauges on the side legs of the encasings

Fig. 15 Sample strain gauge on encasing

This setup includes two rigid reaction plates at its top and bottom that are connected together with four circular columns. Hydraulic jack is located on the lower reaction plate. A loadcell is mounted on the jack using two connecting plates. A 3D view of the test setup is shown in Fig. 13.

To measure displacements in different parts of the specimen, eight LVDTs are installed on the specimen. The net displacement exerted to specimen is measured using two auxiliary bars connected to the two end plates. Properties of each LVDT and its location are shown in Table 5.

Beside LVDTs, six strain gauges are installed on CFRP layers. These strain gauges are installed on the encasing side legs. The location of the strain gauges is shown in Fig. 14. A sample of installed strain gauge on encasing is shown on Fig. 15.

4. Test results and discussion

The test results and the performance of each specimen is presented separately.

4.1 Specimen 1

A view of specimen 1 prior to loading is shown in Fig. 16.

The hysteresis curve of specimen 1 is shown in Fig. 17. The hysteresis loops are stable and symmetric with smooth curves showing positive hardening slope.

The maximum tension adjustment factor (ω) which is the ratio of the maximum tensile force to the nominal yielding force is 1.58. The maximum compression adjustment factor (β) which is the ratio of maximum compressive force to maximum tensile force is 1.11. The maximum displacement ductility (μ) is 24. The ratio of cumulative inelastic axial deformation to the yield deformation (η) of specimen up to the end of $2\Delta_{bm}$ cycle is 431 which satisfies the requirement of AISC 341. Other measured parameters for specimen 1 are presented in Table 6. In each cycle the brace tensile and compressive displacements are divided by the yielding length of the core, and the average tensile and compressive strains (ε_t and ε_c) are obtained.

In order to investigate the performance of the brace when subjected to consecutive cycles and fatigue effects, displacement cycles with constant amplitude of $1.5\Delta_{bm}$ are exerted to the specimen. The specimen withstood 10 cycles without stiffness and strength loss, in the 11 cycle the specimen was loaded in tension until it failed. The load-displacement response of specimen 1 to repeated displacement cycles is shown in Fig. 18.

No evidence of excessive global deformation and curvature was observed in specimen 1. Furthermore, no rupture or debonding was observed in the fibers. The connection of core to the end plates remained elastic and undeformed up to end of test.

The encasing was disassembled to investigate the core. As it is shown in Fig. 19, the failure occurred in the middle of the core in a ductile pattern. Significant reduction in the

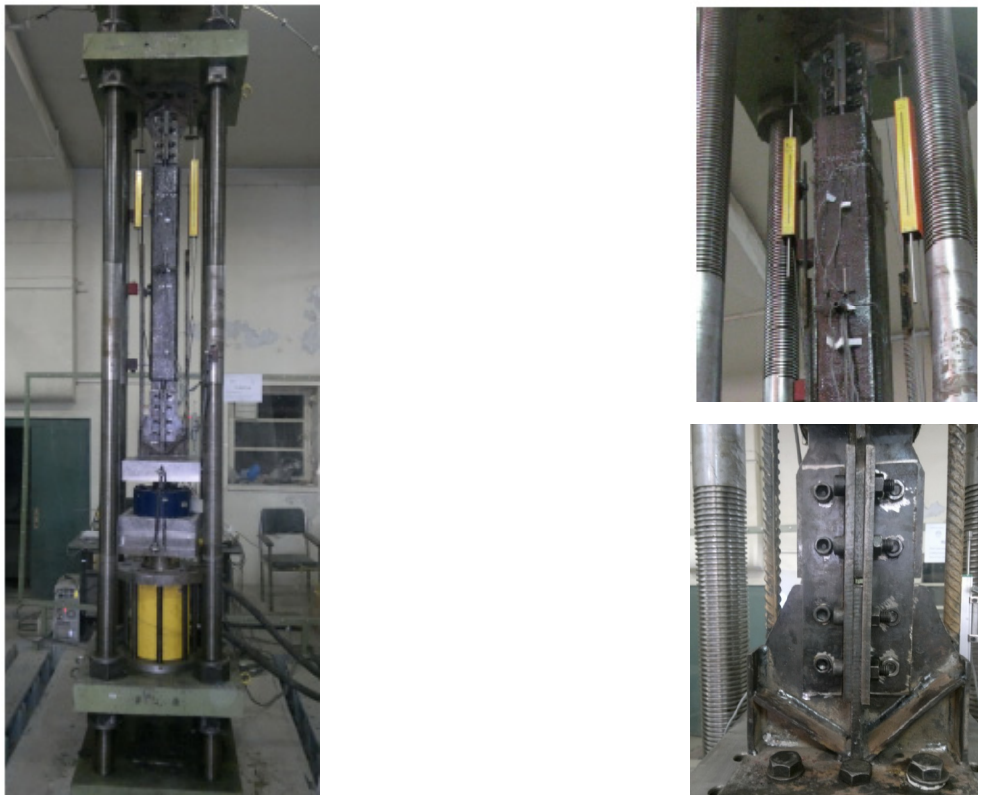

Fig. 16 Specimen 1 in the uniaxial test setup

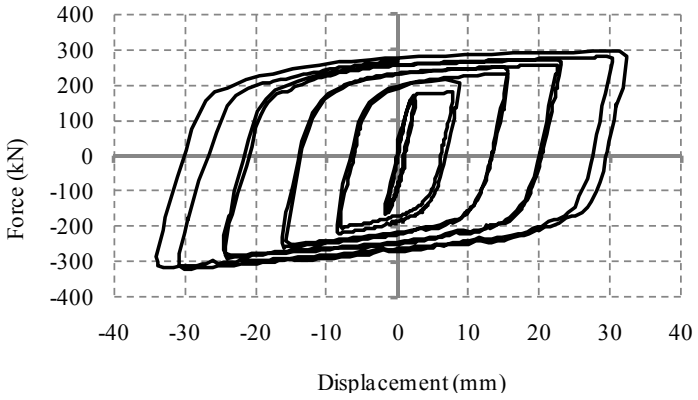

Fig. 17 Load-displacement curve of specimen 1 (AISC 341 protocol)

cross section area and necking is witnessed. The core experienced limited in-plane and numerous out-of-plane higher mode buckling waves.

Higher mode buckling at both ends is more severe than the middle of the core. The number of half-waves due to buckling is 30. Concentration of compressive strains is at ends and concentration of tensile strain is at the middle. Considering the limited amplitude of higher mode buckling at both ends, the middle part of the core necks in repeated cycles of loading and finally fractures. At the ends of the core compressive permanent strain and in the middle of the core permanent tensile strain is observed. The maximum permanent compressive strain in thickness and width of the core is 3.4% and 3.8%, respectively. The maximum permanent tensile strain in the middle of the specimen is

Table 6 Measured parameters of specimen 1

Cycle	ε_t (%)	ε_c (%)	ω	β	$\beta\omega$	μ	η
Δ_y	0.23	0.17	-	-	-	-	-
Δ_y	0.22	0.22	-	-	-	-	-
$0.5\Delta_{bm}$	0.96	0.99	1.03	1.11	1.13	6	19
$0.5\Delta_{bm}$	1.07	1.04	1.15	1.03	1.19	6	41
Δ_{bm}	1.90	1.91	1.26	1.11	1.40	12	83
Δ_{bm}	1.90	1.98	1.36	1.04	1.40	12	126
$1.5\Delta_{bm}$	2.75	2.98	1.48	1.01	1.49	17	189
$1.5\Delta_{bm}$	2.82	2.95	1.49	1.06	1.58	17	253
$2\Delta_{bm}$	3.70	4.14	1.55	1.14	1.76	22	339
$2\Delta_{bm}$	3.95	3.75	1.58	1.09	1.73	24	431

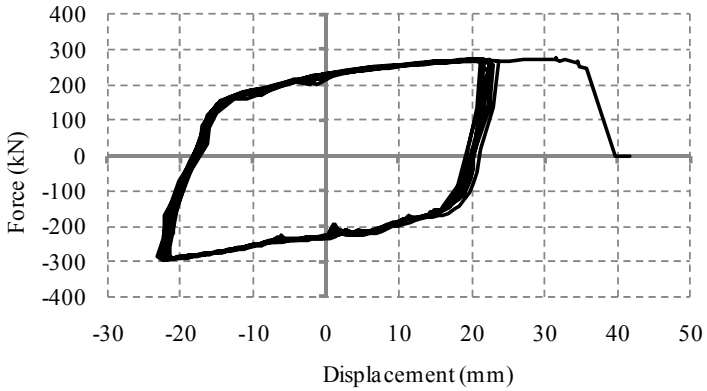

Fig. 18 Load-displacement curve of specimen 1 (fatigue protocol)

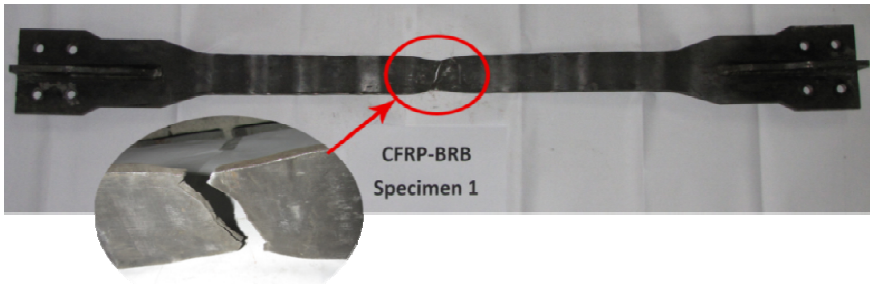

Fig. 19 Core of specimen 1 after test

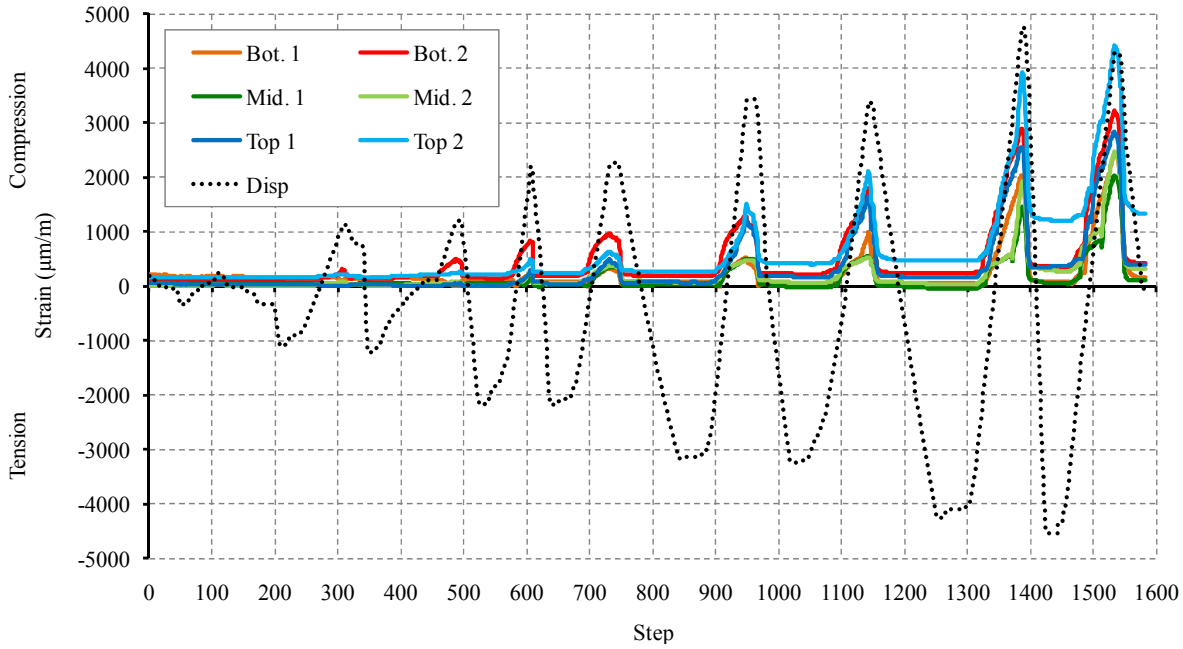

Fig. 20 Strain history of the encasing CFRP (specimen 1)

4.3% and 6.1%, respectively. Data collected from strain gauges of CFRP layers are shown in Fig. 20.

All the strain values are positive revealing the fact that the fibers continuously experience tensile strains. In other words, when specimen is loaded in tensile cycles, values of the strain gauges drops to zero and when the specimen sustain compressive cycles, the gauges show positive values. The two strain gauges installed on each height show close values. The maximum strain of the middle gauges is 2460 μm/m. The maximum strain at the ends of the encasing is 4422 μm/m.

At the end of encasing where the encasing concrete is in contact with the core, crack and spalling was observed which can be attributed to the thrust exerted by the core stiffeners. Local failure at the end of encasing of specimen 1 is shown in Fig. 21.

Fig. 21 Crack growth and local failure at the end of encasing of specimen 1

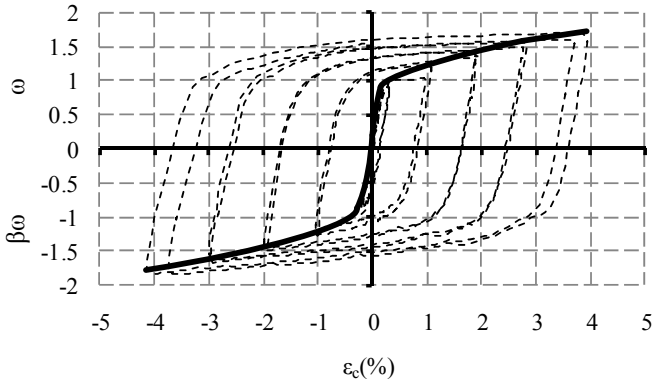

Fig. 22 Envelope curve of hysteresis curve of specimen 1

Fig. 23 Specimen 2 in the uniaxial test setup

The envelope curve of hysteresis curve of specimen 1 is shown in Fig. 22 for design purposes. This curve is normalized for strain percentage and the ratio of axial force to yield force.

4.2 Specimen 2

Concrete defect was observed near the end of encasing of specimen 1. Similar observation is reported in past researches (Tremblay *et al*. 2006, Uang and Nakashima 2004). Owing to the fact that the dimension and volume of the encasing is limited, using longitudinal and transverse reinforcing rebars in order to prevent crack in concrete is not practical. In this research steel fibers are used to increase surface stiffness and tensile strength of encasing concrete. The small size of fibers allows appropriate spread

in the concrete blocks. The main effect of steel fibers on concrete is that fracture, crack initiation and crack growth in concrete are delayed and controlled (ACI 544.1 2002). The steel fibers in specimen 2 are Crimped End Wire of Type I (Cold-Drawn Wire) according to ASTM A820 (2001) with diameter of 1 mm and out to out length of 51 mm. The average tensile strength of wires is obtained 1201 MPa. The fiber content of the mixture is 0.45 percent of the volume of concrete.

Particle size distribution curve in specimen 2 is adjusted to incorporate fine aggregates to prevent fibers from sticking together. Assembled specimen in the test setup is

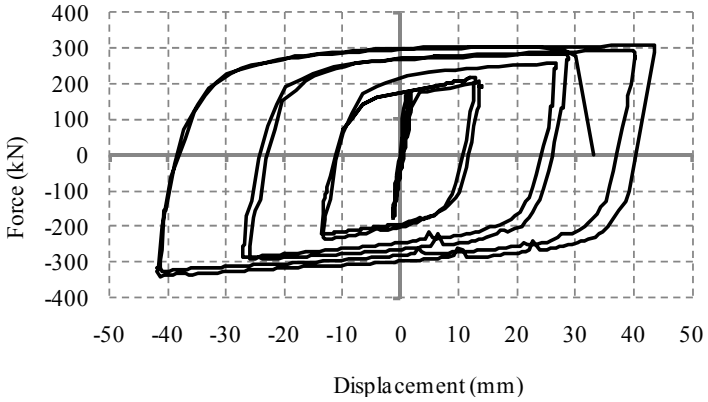

Fig. 24 Load-Displacement curve of specimen 2

Fig. 25 Core of specimen 2 after test

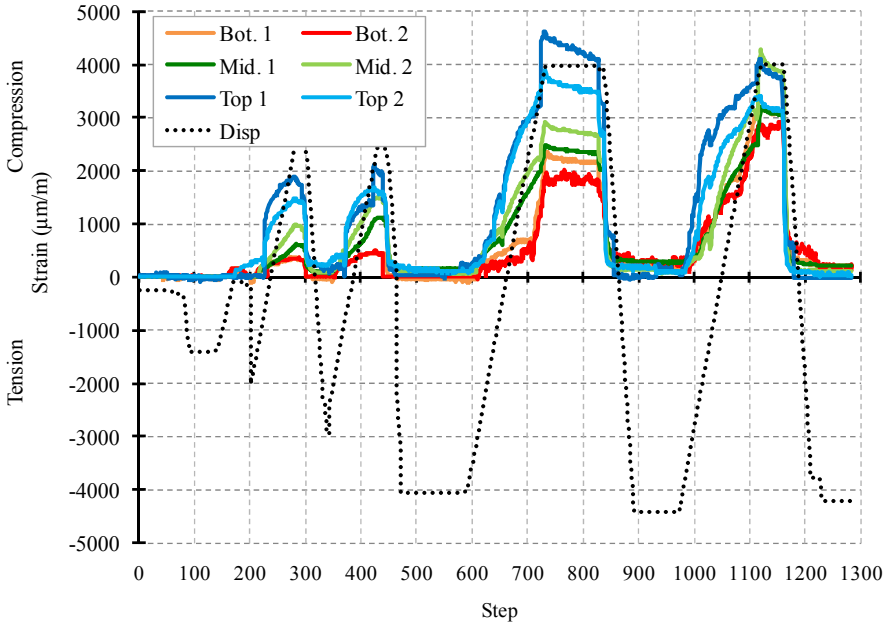

Fig. 26 Strain history of the encasing CFRP (specimen 2)

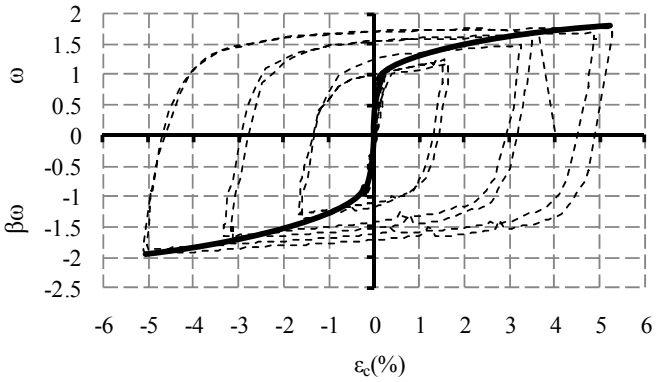

Fig. 27 Envelope curve of hysteresis plot of specimen 2

Table 7 Measured parameters of specimen 2

Cycle	ε_t (%)	ε_c (%)	ω	β	$\beta\omega$	μ	η
Δ_y	0.18	0.06	-	-	-	-	-
Δ_y	0.16	0.21	-	-	-	-	-
$0.5\Delta_{bm}$	1.65	0.05	1.18	1.08	1.28	13	36
$0.5\Delta_{bm}$	1.55	1.65	1.24	1.10	1.37	12	70
Δ_{bm}	3.25	3.32	1.49	1.11	1.66	26	145
Δ_{bm}	3.48	3.15	1.64	1.08	1.76	28	225
$1.5\Delta_{bm}$	4.87	4.99	1.67	1.16	1.93	39	340
$1.5\Delta_{bm}$	5.30	5.02	1.74	1.17	2.04	42	464
$2\Delta_{bm}$	4.02	-	1.49	-	-	32	488
$2\Delta_{bm}$	0.18	0.06	-	-	-	-	-

shown in Fig. 23.

Force-displacement curve of specimen 2 is shown in Fig. 24. As is shown in Fig. 24, the performance of specimen was satisfactory up to the end of second cycle of $1.5\Delta_{bm}$, which is corresponding to strain of 5.30%. Thereafter, when the tensile displacement reached 30 mm the core fractured. The maximum tension and compression adjustment factors in specimen 2 are 1.74 and 1.17, respectively. Also the ratio of cumulative inelastic axial deformation to the yield deformation (η) of specimen until the end of test is 488. The maximum displacement ductility (μ) is 42. The measured parameters of specimen 2 are shown in Table 7.

The strength adjustment factors of specimen 2 are generally greater than specimen 1. The core of specimen 2 is shown in Fig. 26. The number of higher mode buckling waves is 35.

Maximum permanent compressive strain in thickness and width of the core is 7.8% and 2.0%, respectively. Also, maximum permanent tensile strain in the middle of the specimen is 24.3% and 22.0%, respectively, which show larger values compared to specimen 1. Data collected from strain gauges are shown in Fig. 27.

Generally the pattern of results obtained from strain gauges of specimen 2 follows that of specimen 1. Maximum strain of middle gauges is 4200 μm/m, while the maximum strains at both ends of the encasing is 4612 μm/m.

The CFRP remained intact in whole specimen. No evidence of local damage and cracking was observed at the ends of encasing. The application of the proposed steel fibers was satisfactory.

Occurrence of failure in specimen 2 after limited cycles is due to strains with large amplitudes, which implies that for BRBs subjected to severe earthquakes low-cycle fatigue effects. The envelope of the hysteresis curve of specimen 2 is shown in Fig. 27.

5. Conclusions

This study presents the idea of replacing steel tube by CFRP layers in encasing in the form of CFRP-BRB. It specifically explains advantages of the CFRP-BRB such as effective use of concrete, ability to provide variable strength through the length of encasing, prefabrication of concrete encasing blocks, sandwiching the steel core, and accurate adjustment of gap between two encasings. The criteria for designing the encasing of the proposed BRB are introduced and the construction detailing is further explained. Two specimens are uniaxially tested under loading protocols, representing DBE and MCE levels, and the backbone curves are presented for design purposes. The main results of this study can be summarized as follows:

- CFRP layers can effectively integrate the concrete blocks to restrain the steel core against local and global buckling and as a result provide appropriate performance for buckling-restrained braces.
- The performance of specimen 1 shows that up to strains of 3.5% which corresponds to DBE level displacements, the BRB specimen can sustain repeated cycles of deformation after enduring the standard loading protocol.
- In earthquakes levels more severe than DBE when the core strain reaches 5% or higher levels the low-cycle fatigue failure governs the behavior of BRB, which requires special requirements in design and detailing.
- Designing BRBs at MCE levels require adopting higher values of adjustment factors for the out of core components in BRB and other force-controlled elements of structure.
- Using steel fibers in the concrete mix of the

encasing can enhance the performance of encasing against concentrated loads of the core.

Generally applying the CFRP wrapped prefabricated concrete encasing can be advantageous and could lead in BRBs which are sensible alternative to the conventional concrete-filled BRBs.

Acknowledgments

The authors would like to thank Mr. Morteza Fazlollahi for his assistance in the preliminary stages of this research.

References

ACI 544.1 R-96 (2002), State-of-the-Art Report on Fiber Reinforced Concrete; American Concrete Institute.

ACI 440.2 R-08 (2008), Building Code Requirements for Structural Concrete; American Concrete Institute, Farmington Hills, MI, USA.

ACI 318 (2014), Building Code Requirements for Structural Concrete; American Concrete Institute, Farmington Hills, MI, USA.

AISC 341 (2010), Seismic provisions for structural steel buildings; American Institute of Steel Construction, Chicago, IL, USA.

ASCE 7 (2010), Minimum Design Loads for Buildings and Other Structures; American Society of Civil Engineers.

ASCE 41 (2013), Seismic Evaluation and Retrofit of Existing Buildings; American Society of Civil Engineers.

ASTM A820 (2001), Standard Specification for Steel Fibers for Fiber-Reinforced Concrete.

Black, C., Makris, N. and Aiken, I. (2002), "Component testing, stability analysis and characterization of buckling restrained braces", Pacific Earthquake Engineering Research Center, University of California at Berkeley, CA, USA.

Chou, C.C. and Chen, S.Y. (2010), "Subassemblage tests and finite element analyses of sandwiched buckling-restrained braces", *Eng. Struct.*, **32**(8), 2108-2121.

DIN 17100, Steel for general structural purposes: Deutsches Institut für Normung.

Dusicka, P. and Wiley, B. (2008), "Concept of buckling restraint of steel braces with fiber reinforced polymers", *Proceedings of the 2008 Structures Congress*, Vancouver, BC, Canada, April.

Ekiz, E. and El-Tawil, S. (2008), "Restraining steel brace buckling using a carbon fiber-reinforced polymer composite system: Experiments and computational simulation", *J. Compos. Constr.*, **12**(5), 562-569.

El-Tawil, S. and Ekiz, E. (2009), "Inhibiting steel brace buckling using carbon fiber-reinforced polymers: Large-scale tests", *J. Struct. Eng.*, **135**(5), 530-538.

Genna, F. and Gelfi, P. (2012a), "Analysis of the Lateral Thrust in Bolted Steel Buckling-Restrained Braces. I: Experimental and Numerical Results", *J. Struct. Eng.*, **138**, 1231-1243.

Genna, F. and Gelfi, P. (2012b), "Analysis of the Lateral Thrust in Bolted Steel Buckling-Restrained Braces. II: Engineering Analytical Estimates", *J. Struct. Eng.*, **138**, 1244-1254.

Lin, P.C., Tsai, K.C., Wang, K.J., Yu, Y.J., Wei, C.Y., Wu, A.C., Tsai, C.Y., Lin, C.H., Chen, J.C. and Schellenberg, A.H**.** (2011), "Seismic design and hybrid tests of a full-scale three-story buckling-restrained braced frame using welded end connections and thin profile", *Earthq. Eng. Struct. Dyn.*, **41**(5), 1001-1020.

Kakaletsis, D.J. (2016), "Comparative experimental assessment of seismic rehabilitation with CFRP strips and sheets on RC frames", *Eartq. Struct., Int. J.*, **10**(3), 613-628.

Nilson, A., Darwin, D. and Dolan, C.W. (2010), *Design of Concrete Structures*, Mac Graw Hil.

Park, J., Lee, J. and Kim, J. (2012), "Cyclic test of buckling restrained braces composed of square steel rods and steel tube", *Steel Compos. Struct., Int. J.*, **13**(5), 423-436.

Razavi, S.A., Shemshadian, M.E., Mirghaderi, S.R. and Ahlehagh, S. (2011), "Seismic design of buckling restrained braced frames with reduced core length", *Proceedings of Structural Engineering World Congres*, Italy.

Su, L., Li, X. and Wang, Y. (2016), "Experimental study and modelling of CFRP-confined damaged and undamaged square RC columns under cyclic loading", *Steel Compos. Struct., Int. J.*, **21**(2), 411-427.

Tabatabaei, S.A.R., Mirghaderi, S.R. and Hosseini, A. (2014), "Experimental and numerical developing of reduced length buckling-restrained braces", *Eng. Struct.*, **77**, 143-160.

Tremblay, R., Bolduc, P., Neville, R. and DeVall, R. (2006), "Seismic testing and performance of buckling-restrained bracing system", *Can. J. Civil Eng.*, **33**(2), 183-198.

Uang, C.M. and Nakashima, M. (2004), "Steel buckling-restrained braced frames", (Yousef Bozorgnia and Vitelmo V. Bertero Eds.), In: *Earthquake Engineering from Engineering Seismology to Performance Based Engineering*, CRC Press.

Wang, Q. and Shao, Y. (2014), "Compressive performances of concrete filled Square CFRP-Steel Tubes (S-CFRP-CFST)", *Steel Compos. Struct., Int. J.*, **16**(5), 455-480.

Watanabe, A., Hitomi, Y., Saeki, E., Wada, A. and Fujimoto, M. (1988), "Properties of brace encased in buckling-restraining concrete and steel tube", *Proceedings of the 9th World Conference on Earthquake Engineering*, Tokyo-Kyoto, Japan, Volume 4, pp. 719-724.

BU